Understanding the Key Requirements for Ultra-Efficient Sensitisation in Hyperfluorescence OLEDs.

Kleitos Stavrou,* Larissa G. Franca, Andrew Danos, Andrew P. Monkman*

Department of Physics, Durham University, Durham, UK, DH1 3LE.

E-mail: kleitos.stavrou@durham.ac.uk, a.p.monkman@durham.ac.uk

Abstract

Blue OLED technology requires further advancements, and hyperfluorescence (HF) OLEDs have emerged as a promising solution to address stability and colour purity concerns. A key factor influencing the performance of HF-OLEDs is Förster resonance energy transfer (FRET). Here, we investigate the FRET mechanism in blue HF-OLEDs using contrasting TADF sensitisers. We demonstrate that the molecular structure of the sensitiser significantly impacts FRET efficiency, exemplified by the spiro-linked TADF molecule ACRSA. The presence of the rigid spiro-bond minimizes dihedral angle inhomogeneity, suppresses lower energy conformers that exhibit minimal FRET to the terminal emitter. Consequently, FRET efficiency can be optimized to nearly 100%. The photophysical properties of the sensitisers also play a crucial role in HF-OLED performance, and we demonstrate how the properties of a near-ideal sensitiser diverge from an ideal TADF emitters. The sensitiser quantum yield need not be a limiting factor as rapid FRET can effectively outcompete non-radiative processes in HF systems. As a result, blue HF-OLEDs utilizing a greenish sensitiser exhibit a remarkable tripling of external quantum efficiency (~30%) compared to the non-HF devices. This new understanding opens avenues for sensitiser design, indicating that green sensitisers can efficiently pump blue terminal emitters, thus reducing device exciton energies and improving blue OLED stability.

Introduction

Commercial OLEDs still require better blue emitters.[1,2] Even today fluorescent and/or triplet fusion emitters are used for commercial blue OLED pixels, as these materials alone provide acceptable device lifetimes.[3] This is despite their lower achievable efficiency compared to blue phosphorescent or thermally activated delayed fluorescence (TADF) emitters, which are currently limited by either intrinsic emitter instability (for blue phosphorescent emitters) or by the absence of suitable high-triplet host materials (for blue TADF emitters).[4,5] The potential benefits of stable higher-performance blue emitters are even more pressing now because of newly envisioned OLED display architectures, which can exclusively utilise blue pixels with external fluorescent colour conversion layers to give simplified and cheaper fabrication processes towards higher efficiency in low power consumption displays.[6,7] A reductions of 30% power consumption across the majority of display devices used in the future could save more than 400 TWhrs per year in global electricity consumption.

Hyperfluorescent (HF) OLEDs may offer a way to circumvent the limitations of either TADF or phosphorescent blue emitters by using them as sensitisers for separate terminal emitters,[8] but this approach is still relative immature and not well understood.[9–11] Typically, efficient blue HF-OLEDs use a high-performance deep-blue sensitiser with good spectral overlap to a terminal emitter, which enables rapid Förster resonance energy transfer (FRET) after efficient harvesting of triplet excitons.[10,12,13] The broad emission spectra and low radiative rates of TADF sensitiser can thus be compensated for by fast and narrowband emission from the terminal emitter, while retaining high utilisation of triplet excitons by the former.[14–16] Lowering the relevant singlet and triplet energies in the emissive layer of the OLED can also improve device stability, and the use of specific narrowband terminal emitters can even allow green-emitting sensitisers to support blue HF-OLED emission.[17]

In the years since the introduction of the basic HF concept, many reports have featured HF-TADF OLEDs with external quantum efficiencies (EQEs) remaining surprisingly lower than their TADF counterparts.[12,18] In other cases, the HF-OLED EQEs are higher,[10,19] without any clear pattern or identifiable underlying cause for these differences. With the introduction of multiresonance (MR) TADF emitters[14] and their ability to also harvest triplet excitons as terminal emitters, the performance of HF-OLEDs typically surpasses that of non-HF devices[20–24] but the internal processes become yet more complicated compared to conventional fluorescent emitters. Similarly to EQE, in many cases the HF-OLED efficiency roll-off

https://doi.org/10.26434/chemrxiv-2023-vnk7q **ORCID:** https://orcid.org/0000-0001-5868-3324

performance is better, but in some cases it is worse.[15,24] We note that in almost all reports researchers use their 'best' TADF emitters in pre-optimised OLED stacks and then simply add a small concentration of the terminal emitter, which is *prima facie* a sensible strategy.[12,25–27] This practice however also gives some clues as to why HF-OLED performance is not always better; the TADF emitter may already be performing at its maximum potential, and introduction of a terminal emitter opens up additional loss pathways such as through charge trapping or triplet migration onto the terminal emitter. While the terminal emitter can itself sometimes contribute to higher performance through higher photoluminescence quantum yields (PLQYs) or horizontally aligned emission dipoles (that improve light outcoupling), these evidently are not always able to outweigh these additional introduced loss pathways.[16,28]

As an additional consideration, these 'best' TADF emitters chosen for use as HF-OLED sensitisers have their performance evaluated initially in TADF-only devices. For donor-acceptor TADF emitters though, it is now well-established that their performance relies on a delicately balanced HOMO-LUMO overlap.[29] Too much overlap will increase oscillator strength and PLQY (itself the ratio of radiative and nonradiative decay rates), but is detrimental to reverse intersystem crossing (rISC) and triplet harvesting. Too little overlap can result in large rISC rates, but limits the PLQY.[30] It therefore seems impossible for D-A TADF emitters with the fastest rISC rates (hence limited PLQYs) to produce high-performance OLEDs by themselves, and so these materials typically are not investigated in HF-OLEDs. Counterintuitively, in HF-OLEDs the PLQY of the sensitiser is not so crucial as long as the FRET rate (k_{FRET}) outcompetes the nonradiative decay, and instead the highest rISC rate is the key parameter that should be valued. However, candidate TADF emitters with such properties will likely be overlooked for HF-OLED applications due to limited intrinsic performance. Indeed, we suggest that many high-performance HF combinations go undiscovered due to this inappropriate self-selection effect.

Identifying this 'blind-spot' in current HF-OLED research, in this work we demonstrate extraordinary HF-OLED performance enhancement by TADF molecules used as sensitisers, which themselves only give moderate non-HF device performance. Starting from our recent work using the high-performance TADF emitter **DMAC-TRZ** as a benchmark,[17,31] we find that despite the lower non-HF device performance of **ACRSA**, the latter enjoys a considerable performance boost in HF-OLEDs, with an almost tripling of the EQE_{max}.[10,32] Similar results are also obtained using the recently reported deeper blue TADF emitter **AZB-TRZ**,[33] which exhibits very fast rISC but is intrinsically limited by low PLQY. Surprisingly, despite the photoluminescence spectra of **ACRSA** and **DMAC-TRZ** being energetically similar, **ACRSA** exhibits significantly higher overall FRET efficiency in HF systems, even when compared to the deeper blue **AZB-TRZ** sensitizer which has better FRET spectral overlap. This unexpectedly complete energy transfer arises as a result of **ACRSA**s rigid structure and very long-lived excited states, which are normally a detriment in OLEDs. These findings establish new and unexpected design rules for high-performance HF sensitisers, that would otherwise go unnoticed.

Results

Photophysics

The steady-state photoluminescence (PL) spectra of **ACRSA** and **DMAC-TRZ** at 10 wt% in mCBPCN host are shown in Figure **1**. **DMAC-TRZ:**mCBPCN films exhibits one strong emission band centred at 500 nm which we have shown is attributed to ^{1}CT emission from its highly twisted quasi-equatorial conformer.[17] Importantly, the intrinsic broadness of the CT photoluminescence (PL) spectrum is due to a sum of PL contributions from different molecular configurations with different D-A dihedral angles in the film, together with some aggregate emission.[34,35] These contributions have different radiative lifetimes and rISC rates as well as spectra, and can be seen independently in time-resolved spectra even when FRET to a terminal emitter is active (in this case **ν-DABNA**)[14,27] (Figure **S1c**). In **ACRSA:**mCBPCN film dual emission is observed in the PL spectrum. The higher energy band at ~400 nm comes from the mCBPCN host (excitation 355 nm), as the **ACRSA** absorption in the region is very weak. The broader emission band at ~500 nm is characteristic of **ACRSA** ^{1}CT emission in solid-state hosts.[36] For this work the **ACRSA** PL spectrum was deconvolved considering three Gaussian contributions (Figure **S2**) corresponding to i) mCBPCN at 400 nm; ii) **ACRSA** ^{1}CT at 497 nm; and iii) **ACRSA** aggregate contributions at 545 nm. The absence of dihedral angle inhomogeneity in **ACRSA** results in a narrower monomer PL spectrum as seen in the deconvoluted spectra of **ACRSA** and reported previously.[35,36]

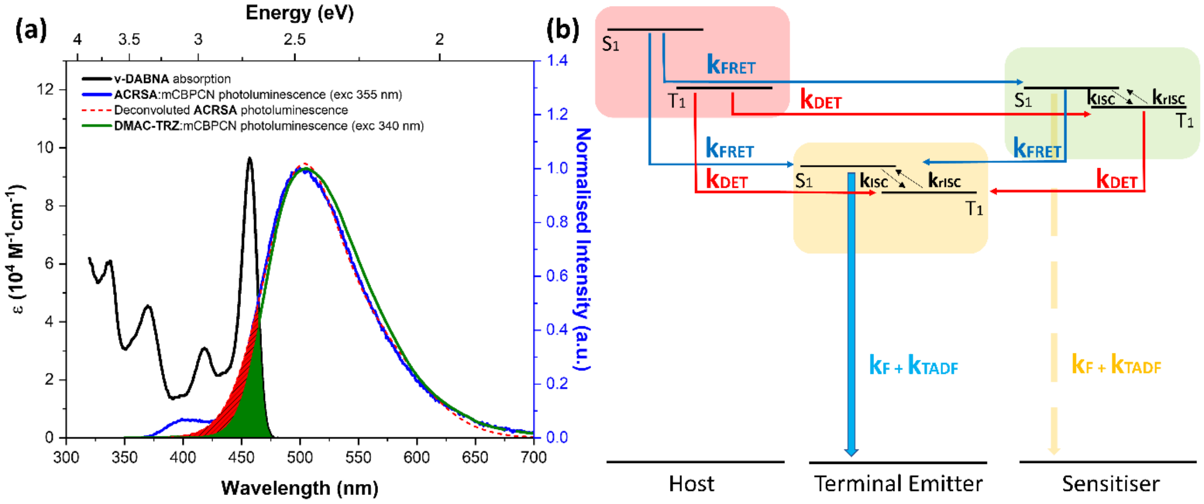

Figure 1: (a) Steady-state absorption of **v-DABNA** in toluene solution, alongside photoluminescence spectra of **ACRSA**:mCBPCN (10% wt) and **DMAC-TRZ**:mCBPCN (10% wt) films, excited at 355 and 340 nm respectively. The filled areas are the spectral overlaps between the curves used to analyse the FRET radius. (b) FRET mechanism in a guest:sensitiser:terminal emitter system. Emission from the sensitiser (Yellow arrow) occurs when FRET is significantly less than 100% efficient.

Excluding the mCBPCN contribution to the **ACRSA** PL spectrum and comparing the spectral overlap in the two TADF emitters with **v-DABNA** absorption,[27] **ACRSA** as sensitiser displays slightly increased spectral overlap because of its higher energy PL onset, highlighted by the red-filled area in Figure **1**, with **DMAC-TRZ** overlap highlighted green. For both emitters only the very blue edge of the highest energy sensitiser emission overlaps with the narrow S_0-S_1 absorption transition of **v-DABNA**, but efficient FRET surprisingly still ensues for both materials (although for different reasons, *vide infra*). The calculated FRET radii between the sensitisers and the terminal emitter are 2.8 nm and 3.2 nm for **ACRSA** and **DMAC-TRZ** respectively (for more details see supporting information). Despite the slightly better spectral overlap of **ACRSA** with **v-DABNA**, the calculated FRET radius is lower compared to **DMAC-TRZ** because the **ACRSA** PLQY is 3 times smaller.

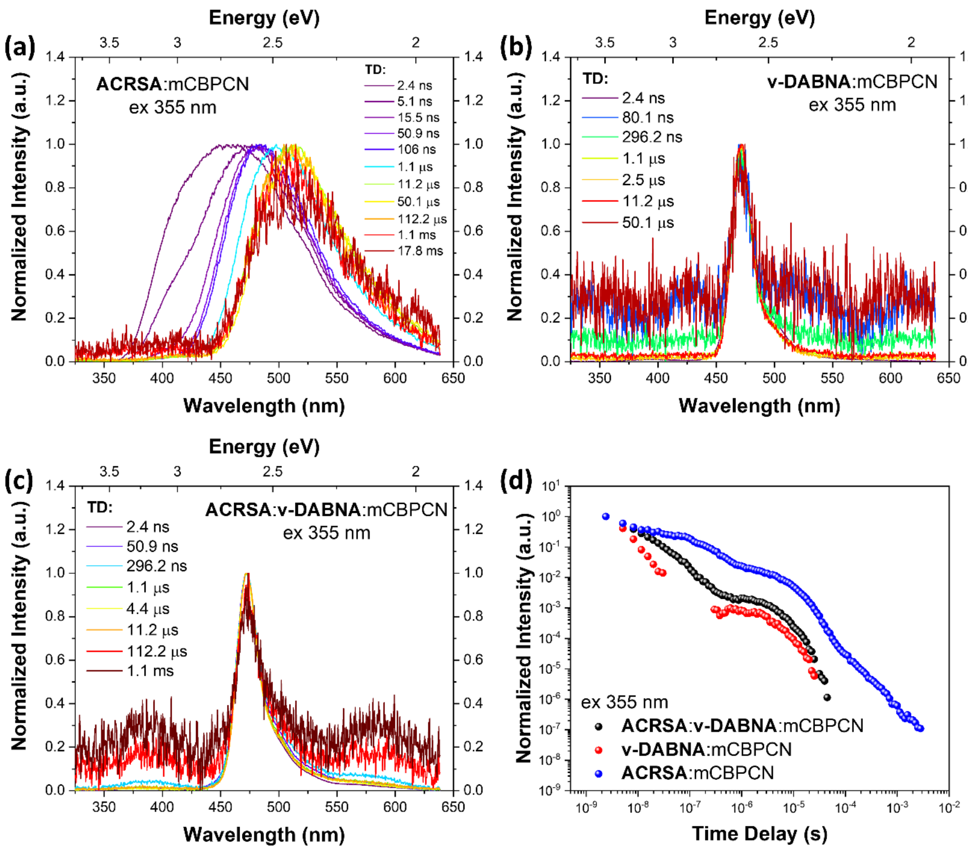

Figure 2: Time-resolved photoluminescence spectra of: (a) **ACRSA**:mCBPCN (10%), (b) **v-DABNA**:mCBPCN (1%) and (c) **ACRSA**:**v-DABNA**:mCBPCN (10:1:89 wt%). (d) Photoluminescence decay traces of the evaporated films at room temperature. λ_{exc}= 355 nm.

The FRET dynamics in the two HF systems were investigated using time-resolved emission spectroscopy. Figure **2a** shows the time-resolved spectra of **ACRSA**:mCBPCN (10 wt%) film at room temperature. As mentioned above in the context of the deconvolution of the steady-state spectrum, three resolvable species contribute to the overall emission. These are the mCBPCN itself, **ACRSA** ^{1}CT, and **ACRSA** excimers, which have lifetimes of 2.95 ns, 322 ns, and 7.9 µs respectively (Table **1**). The unusually long ^{1}CT decay lifetime arises from the highly decoupled nature of the spiro-linked **ACRSA** D-A units,[37] and becomes crucially important for its use as a sensitiser in HF systems as discussed below. With the additional presence of 1 wt% **v-DABNA**, the prompt fluorescence (PF) lifetime has two components. Direct (355 nm) excitation of **v-DABNA** leads to a component of emission with a lifetime of 3.5 ns, the same as **v-DABNA** in mCBPCN. Exciting the HF film at 420 nm (selective **v-DABNA** excitation) also produces the same emission decay kinetics as a film without **ACRSA** sensitiser (Figure **S3**). The FRET-accelerated PF lifetime of **ACRSA** in the HF film reduces from 322ns to 39.27 ns (Table **1**). To put this significant **ACRSA** emission lifetime quenching into context, the PF lifetime of **DMAC-TRZ** in mCBPCN is 21.66 ns and reduces to 15.55 ns with the introduction of 1 wt% **ν-DABNA**. This has an enormous impact on the FRET efficiency (n_{FRET}) and subsequent HF-OLED performance of this system (Table **S1**).

Table 1. Key photophysical characteristics of **ACRSA**:**ν-DABNA:**mCBPCN, **ACRSA**:mCBPCN and **ν-DABNA**:mCBPCN, films at room temperature. λ_{exc} = 355 nm.

Photophysical characteristics	**ACRSA:ν-DABNA:mCBPCN** (HF)	**ACRSA:mCBPCN** (Sensitiser only)	**ν-DABNA:mCBPCN** (Terminal emitter only)
Concentration (wt%)	10 : 1 : 89	10: 90	1: 99
$^{a}\lambda_{max}$ (nm)	476	500	477
^{a}FWHM (nm)	17.7	96.1	17.5
$^{b}\Phi_{PL}$ (%)	66.1	30.7	60.9
$^{c}\tau_{LE}$ Host(ns)	3.5 (ν-DABNA)	2.95	-
$^{c}\tau_{PF,1}$ (ns)/(A_{PF})	15.99 (78%)	72.1 (60%)	3.5
$^{c}\tau_{PF,2}$ (ns)	60.93 (22%)	391.14 (40%)	-
$^{d}\tau_{PF,av}$ (ns)	39.27	322.03	3.5
$^{c}\tau_{DF}$ (μs)	4.5	7.9	4.6

[a] Values were obtained from the steady-state photoluminescence spectra. [b] Photoluminescence quantum yield (Φ_{PL}) under N_2, excited at 355 nm. [c] Lifetimes were obtained by fitting monoexponential and biexponential functions. [d] Average lifetime $\tau_{PF,av}=(A_{PF,1}*\tau_{PF,1}^{2}+A_{PF,2}*\tau_{PF,2}^{2})/(A_{PF,1}*\tau_{PF,1}+A_{PF,2}*\tau_{PF,2})$.

The k_{FRET} and n_{FRET} of the HF systems can be estimated from the changes in sensitiser PF lifetime in the presence and absence of the terminal emitter (see FRET equations section in supporting information).[9] In the **ACRSA** HF system, the n_{FRET} is calculated to be 87.8%, which is very high given such a limited spectral overlap between the sensitiser and terminal emitter (Figure **1**). In the **DMAC-TRZ** HF system the n_{FRET} is instead calculated to be 28.2%. This later value is obviously at odds with the photoluminescence and previously reported electroluminescence (EL) spectra of the HF-OLEDs, because we have so far only considered the quasi-equatorial conformer emission from **DMAC-TRZ**.[17] Additional FRET from the recently established quasi-axial conformer to the terminal emitter (that otherwise undergoes energy transfer to the lower energy quasi-equatorial conformer) means that the FRET radius, k_{FRET} and n_{FRET} are larger in the actual **DMAC-TRZ:ν-DABNA** HF system (for more information see estimation of FRET properties in ESI).[17]

While an unexpected conformer explains the surprisingly small calculated n_{FRET} for **DMAC-TRZ**, this cannot be the case for conformationally rigid **ACRSA**. Instead, we propose that the very long ^{1}CT emission lifetime provides an ample window of opportunity for relatively slow FRET to achieve high n_{FRET}. Indeed, considering the rate constants derived from the emission decays,[38] we arrive at a k_{FRET} for the **ACRSA** HF system of 2.24×10^{7} s^{-1}, and a very similar value for the **DMAC-TRZ** HF system (1.81×10^{7} s^{-1}). In **DMAC-TRZ** this k_{FRET} is in direct competition with intersystem crossing rate ($k_{ISC} = 2.2 \times 10^{7}$ s^{-1}) and fluorescence rate ($k_f = 2.07 \times 10^7$ s^{-1}, Table **S4**), and from the large PLQY of **DMAC-TRZ** the non-radiative rates are already known to be small.[39] In **ACRSA** k_{ISC} and k_f are both much slower, 1×10^6 s^{-1} and 3.1×10^6 s^{-1} respectively. Non-radiative rates must also be slow to support such long singlet exciton lifetimes in this emitter, thus allowing FRET to dominate far beyond what it can achieve with **DMAC-TRZ**, despite the similar k_{FRET} values. To generalize, sensitisers with slow radiative *and* slow non-radiative rates provide enough time for k_{FRET} to accumulate and dominate the exciton dynamics, even though these properties by themselves limit the potential performance of the sensitiser as a TADF emitter in its own right.

We also note that the calculated η_{FRET} represent the probability for singlet energy transfer across a single exciton lifetime. While this is appropriate for standard FRET between fluorescent materials, if the exciton is instead cycling (in some cases multiple times) between singlet and triplet states (as in a TADF sensitizer), the overall/cumulative chance of undergoing FRET increases significantly with each cycle. Here, we estimate η_{FRET} using only the prompt lifetimes, thus TADF materials with fast rISC rate and high DF/PF ratio will have a much higher cumulative FRET efficiency. These high cumulative FRET efficiencies are then what is observed when considering emission intensities of sensitiser and terminal emitter in film PL or device EL spectra, which in some cases indicate far more complete FRET than the calculated η_{FRET} would otherwise imply (*vide infra*).

Table 2: FRET properties of the hyperfluorescence systems.

FRET properties	**ACRSA: ν-DABNA:mCBPCN**	****DMAC-TRZ: ν-DABNA:mCBPCN**	**AZB-TRZ: ν-DABNA:mCBPCN**
FRET radius, R_0 (nm)	2.80	3.21	3.22
FRET efficiency (%)	87	28	37
FRET rate ($\times 10^7$ s^{-1})	2.24	1.81	2.46
Average distance, r (nm)*	2.02	3.75	3.51

*All hyperfluorescence studies use wt% concentrations, thus the real number of sensitiser molecules in the film will depend on their molecular weight. Thus **ACRSA**, that has the smaller molecular weight, will have much higher number of molecules in the film compared to **DMAC-TRZ** and **AZB-TRZ** (Table **S3**) and smaller average distance.

** considering the quasi-equatorial conformer only

An additional factor contributing to the small calculated η_{FRET} in the **DMAC-TRZ** HF system is the significant emission contribution from lower energy conformers, evident in the late PF and early delayed fluorescence (DF) regime in the time-resolved spectra (Time delay 20 - 5000 ns, Figure **S1c, d**).[34] While not significantly detrimental in **DMAC-TRZ** OLEDs, these low-energy emitting conformers have vanishing spectra overlap with **ν-DABNA** resulting in a subset of **DMAC-TRZ** molecules trapped in molecular geometries with poor n_{FRET}. As a result, the surprisingly low calculated **DMAC-TRZ** n_{FRET} using the PF decay rates is very much an average representing a broad underlying distribution of conformers. The **ACRSA** HF system does not have a comparable broad distribution of conformers contributing to the time-resolved decay (Figure **2c**), such that all excited states experience similar n_{FRET} with no ensemble averaging. This comparison highlights how homogenous emitter conformations in TADF materials, while already known to be advantageous in standard OLEDs, also yield key benefits in HF-OLEDs by supporting more complete FRET.

The DF regime is also important to consider for HF systems, as rISC controls triplet exciton harvesting and lifetimes that support high efficiency in devices. The **ACRSA** HF system has a DF lifetime of 4.5 μs, which appears to match that of **ν-DABNA**:mCBPCN (Table **1**), while the **ACRSA** non-HF system has a DF lifetime of 7.9 μs, which is influenced by excimer states. For comparison, **ACRSA** at 1wt% loading in zeonex or DPEPO films has DF lifetimes of 6.3 μs and 7.3 μs respectively with no excimer emission observed. At 10 wt% in DPEPO host, and similarly to mCBPCN host, the **ACRSA** DF lifetime is 8.7 μs with clear excimer emission observed.[36] This implies that all of the **ACRSA** triplet population that was formed by ISC in the HF film, is successfully up-converted and transferred to the terminal emitter. **ACRSA** excimer emission, which appears to be dominant in **ACRSA**:mCBPCN DF at 10 wt%, disappears completely in the HF system despite the high **ACRSA** concentration. This comparison shows that the presence of the terminal emitter in the **ACRSA** HF system prevents excitons forming excimers, with FRET outcompeting the formation rate.

The **DMAC-TRZ** HF system DF is however divided in different time regimes (Figure **S1**). Initially, there is a fast component in the early DF regime (~ 500 ns) with high contribution to the time-resolved PL emission from the highly twisted **DMAC-TRZ** conformers (emission at 510 nm) that have limited overlap with the terminal emitter and thus low n_{FRET} (Figure **S1d**). The second regime is similar to the **ν-DABNA**:mCBPCN film DF, where efficient FRET occurs, and the last regime is an extension of the DF tail which comes from the slow up-conversion of unfavourable species in the inhomogeneous **DMAC-TRZ** system (less twisted conformers with slow k_{rISC}). The average DF lifetime is 11 μs (Table **S1**), indicating that these slow species greatly increase the overall DF lifetime of the hyperfluorescent system, an undesirable phenomenon in OLEDs.

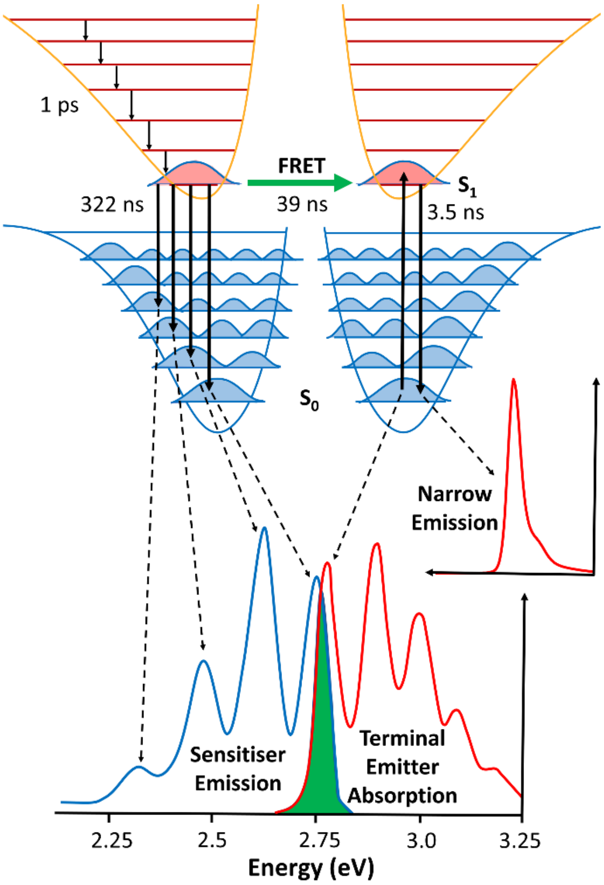

Figure 3. Schematic energy level diagram for FRET between a hypothetical TADF sensitiser and **ν-DABNA** terminal emitter, showing how a very small spectral overlap can still give rise to fast and efficient energy transfer between them. FRET is relatively slow because the sensitiser (singlet CT state) transition dipole moment is very small. Thus, the dipole-dipole interaction is weak, such that we are in the weak coupling (FRET) regime.

The above indicates that for a (conformationally) homogeneous hyperfluorescent sensitiser i.e. **ACRSA**, the FRET requirements to achieve high efficiency sensitisation are not as previously understood. As seen from the comparison of **ACRSA** emission to **ν-DABNA** absorption spectra, Figure **1**, the spectral overlap for this hyperfluorescent system is extremely small, but this does not ultimately limit n_{FRET}. This realisation is very important for OLED applications, as it allows us to maintain efficient cumulative FRET while also minimising the excitation energy of the sensitiser as much as possible. This consideration is not something unique to **ACRSA** but arises from the fortuitous photophysical properties of the energy donor and acceptor, depicted in Figure **3**. In **ν-DABNA** the S_0-S_1 transition has a very high oscillator strength and very narrow bandwidth. For the energy donor (sensitiser) the vast majority of singlet excited state population resides in the S_1 0-0 vibrational state as the radiative lifetime is long compared to internal conversion. Thus, the overlap between the populated energy donor states and the spectrally narrow energy acceptor (terminal emitter) absorption band remains suitably strong. Overlap of just the red edge of the acceptor absorption with the blue edge of the donor emission still ensures that all of the donor population can be transferred to the acceptor. This is all that is required to couple all the donor excited state population to the acceptor making the **ACRSA**:**ν-DABNA** hyperfluorescent system an ideal situation for maximal n_{FRET} despite minimal spectral overlap. As a result, the lowest possible sensitiser singlet excited state energy, and therefore lowest triplet energy as well can still be used for blue OLED emission, increasing the range of usable host and emitter materials considerably. This realisation redefines the photophysical design requirements for sensitiser and terminal emitter to achieve optimal FRET with minimal sensitiser excited state energy for HF-OLEDs.

Devices

Turning to HF-OLEDs, it is well established that slow rISC in MR-TADF materials such as **ν-DABNA** leads to unsatisfactory efficiency roll off at higher current densities in devices, as we observe here (Figure **4d-f**). As expected from previous reports,[10,32] **ACRSA** does not perform as strongly in OLEDs as **DMAC-TRZ**. In our device stack the EQE_{max} is limited to ~11% for this emitter compared to ~25% for **DMAC-TRZ**, both at 10 wt% concentration in mCBPCN host and largely a result of **ACRSA**'s low PLQY and slow radiative decay rate (with slow PF). The roll-off for **ACRSA** is also worse than in **DMAC-TRZ** OLEDs, a result of its slower rISC and longer exciton lifetimes (Table **S4**). Although the rISC rate of **ACRSA** is not much lower compared to the average rISC rate of **DMAC-TRZ**, we also note that the k_{rISC} of the fastest **DMAC-TRZ** conformers is almost an order of magnitude larger (Figure **S6**). For these reasons, it is understandable why **ACRSA** has not been widely investigated for high-performance HF-OLEDs.

Surprisingly though, upon introduction of 1 wt% **ν-DABNA** the EQE_{max} of the **ACRSA** device almost triples to 28.5%. In striking contrast, the **DMAC-TRZ** HF-OLEDs retain nearly identical performance to **DMAC-TRZ** alone (Figure **4**). Furthermore, despite the similar EL spectra of **ACRSA** and **DMAC-TRZ** OLEDs, the FRET is significantly more complete in the **ACRSA** HF-OLEDs, as evidenced by its EL spectra being identical to that of **ν-DABNA**, Figure **4c**. Significant residual sensitiser emission is observed in the **DMAC-TRZ** HF-OLED.

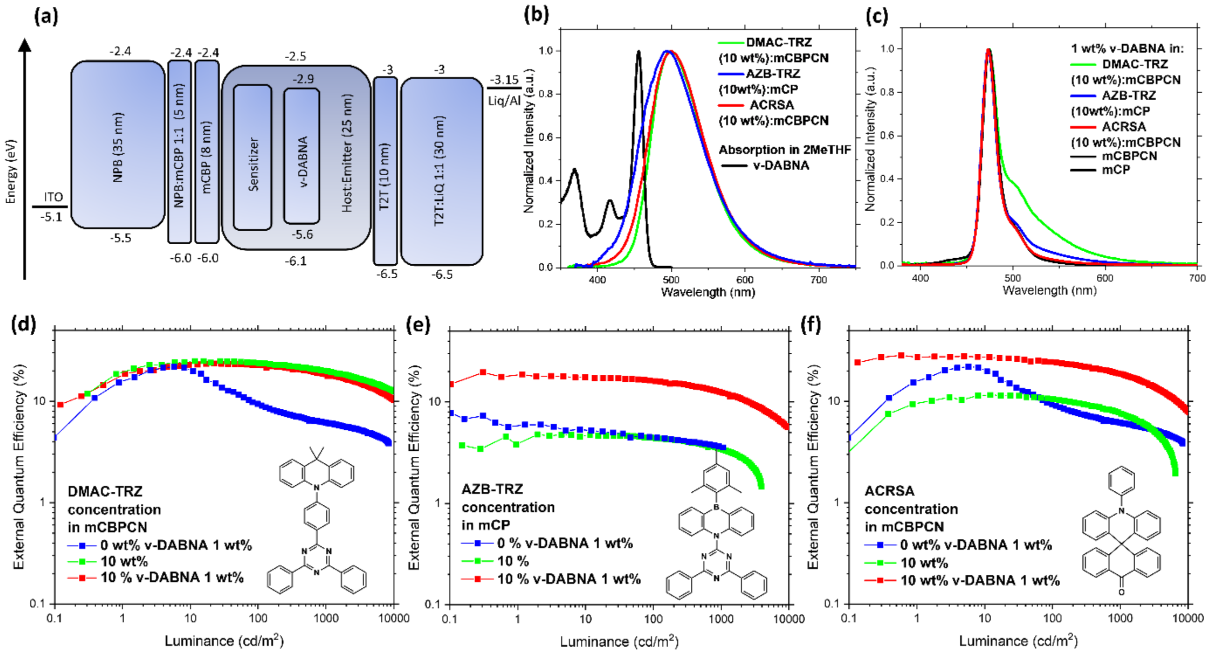

Figure 4. OLEDs performance. (a) Device architecture and electroluminescence spectra of (b) TADF devices, (c) HF-OLEDs. EQE versus luminance of (d) **DMAC-TRZ**, (e) **AZB-TRZ** and (f) **ACRSA** OLEDs with and without the terminal emitter (blue curve **v-DABNA** without the presence of the sensitiser for comparison)

We propose that this contrasting behaviour - with **ACRSA** enjoying significantly greater performance *enhancement* in the HF-OLEDs - actually arises due to the same properties that make **ACRSA** a less effective TADF emitter. In particular, the slow radiative and non-radiative/ISC rates of **ACRSA** are both extensively outcompeted by FRET to **v-DABNA**, largely obviating the disadvantages of its low PLQY. This long window of opportunity for energy transfer, as well as the absence of any unfavourable conformers having poor η_{FRET} (enforced by the rigid spiro-centre) means that FRET can be far more complete for **ACRSA:v-DABNA** than might otherwise be expected. In contrast, k_{ISC} and k_F are comparably fast in **DMAC-TRZ**, leading to less complete FRET despite similar spectral overlap (see J factors in Table **S3**). The high PLQY in **DMAC-TRZ** also means that radiative decay already outcompetes nonradiative decay, and so there is little headroom for additional FRET processes to improve the device performance further. There also exists a sub-population of **DMAC-TRZ** molecules in unfavourable configurations, with redshifted emission making these inaccessible for FRET.

In addition to the above, the similar EQE roll-off in the **ACRSA** TADF and HF devices indicate that triplet harvesting remains the exclusive role of the sensitiser, and is not significantly impacted by the presence or absence of the **v-DABNA** terminal emitter. Nonetheless the roll-off slope is improved at high luminance, indicating that the HF-OLED likely helps reduce the accumulation of excitons by providing rapid FRET and emission pathways. We again note that the ability to achieve efficient FRET even with significantly low energy emitters (like **ACRSA**) opens up new possibilities for enhancing the lifetime of blue HF-OLEDs. Rather than relying on deep-blue emitters and associated high-triplet hosts,[4,5,15] green emitting TADF sensitisers and their lower-triplet hosts can be significantly more stable in devices. This stability is due to both the wider choice of chemical groups usable at these energies (for both hosts and emitters), as well as the smaller exciton energies. Combined with the highly absorbing red edge of the terminal emitter (already effectively optimised for **ν-DABNA**), this surprising effectiveness of HF systems with seemingly inadequate FRET overlap demonstrates a way to achieve highly efficient and stable blue OLEDs, using attractive and well-developed green-emitting sensitisers.

To explore this strategy further, we investigated an additional non-rigid TADF molecule, with blue-shifted emission compared to **DMAC-TRZ**. **AZB-TRZ** (Figure **4e**) has a considerably different balance of decay rates compared to **ACRSA** and **DMAC-TRZ**, with its intrinsic performance limited instead by a fast non-radiative decay rate and low PLQY (Table **S2**).[33] Similar to **DMAC-TRZ**, a clear distribution of dihedral angles is observed through the time dependent emission spectra (Figure **S5a**) leading to limited spectral overlap of specific conformers (redshifted species) with the terminal emitter. The spectral overlap of the steady-state emission spectra with **ν-DABNA** is nonetheless higher compared to **ACRSA** and **DMAC-TRZ** sensitisers (Figure **S4**), leading to the highest J factor (Table **S3**) and FRET radius (Table **2**) in this series of sensitisers.

Not surprisingly, the CT energy dispersion together with fast k_F and k_{ISC} of **AZB-TRZ** competes with the k_{FRET} (Table **2**) leading to a seemingly low calculated n_{FRET} of 37%, but also more significant population of the triplet state. The latter indicates why n_{FRET} appears to be underestimated when considering the near-complete energy transfer apparent from the HF-OLED spectra, i.e. small contribution from the sensitiser to the EL spectrum. As mentioned above, ISC/rISC cycling can depopulated and repopulate the singlet state (potentially multiple times) before emitting, and FRET will also occur during the DF/triplet regime. The calculated n_{FRET} from the PF decays represents the probability of FRET without considering these cycling events, rather than the larger cumulative n_{FRET} over the entire exciton lifetime.

A combination of FRET and fast rISC therefore together help to significantly enhance the **AZB-TRZ** device efficiency, although we note that the energy transfer is not as complete as in **ACRSA** and a small **AZB-TRZ** emission contribution is observed in the EL spectrum (~ 510 nm, Figure **4c**). Indeed, the fast radiative and non-radiative singlet decay rates do not allow

FRET to completely dominate the exciton dynamics for this TADF sensitiser, and the colour coordinate does not shift as much into the blue as for the **ACRSA** HF-OLEDs, surprisingly despite **AZB-TRZ** having higher energy emission and better spectral overlap (Figure **5**). The device EQE_{max} nonetheless almost quadruples, rising from 5 to 20%, and the excellent roll-off afforded by the rapid rISC of **AZB-TRZ** helps preserve and even enhance excellent roll-off performance in the HF devices compared to the TADF devices. This case therefore represents a near-ideal case study of the advantages of HF-OLEDs, with a highly effective sensitiser providing exceptionally fast triplet up-conversion to a near-ideal terminal emitter.

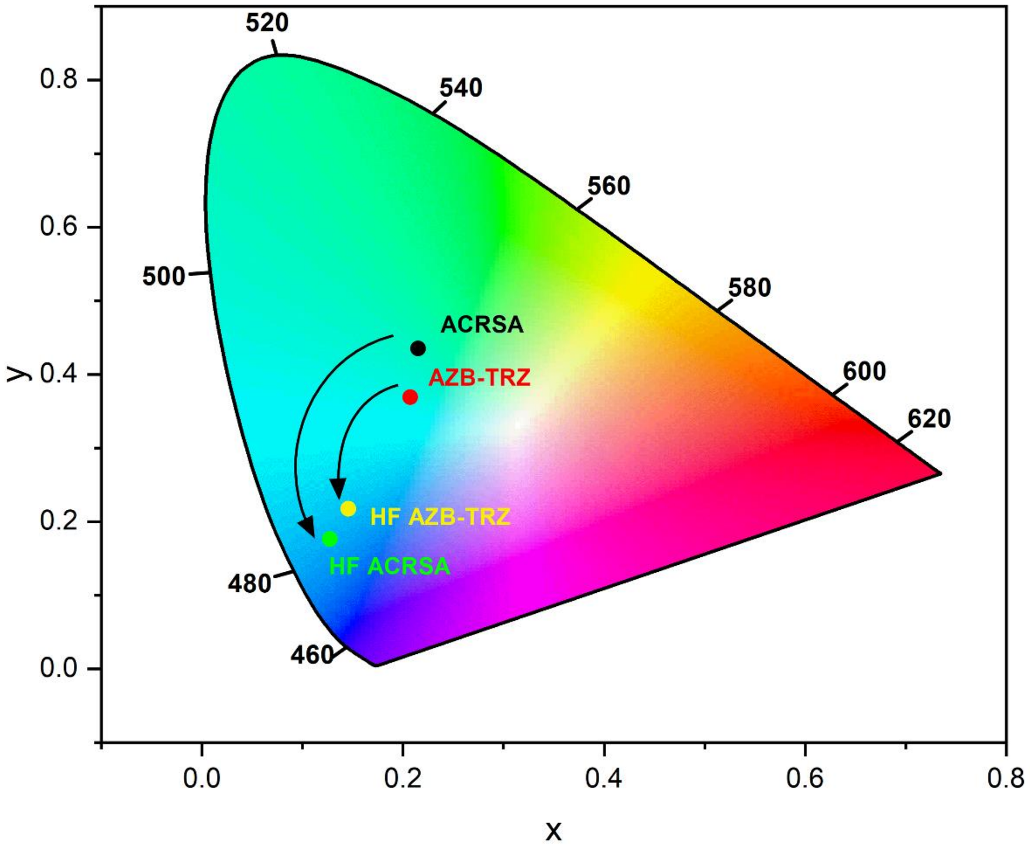

Figure 5. Comparison of CIE coordinates of **ACRSA** and **AZB-TRZ** OLEDs and HF-OLEDs, collected at 1000 cd m^{-2}.

The performance of **ACRSA** and **AZB-TRZ** HF-OLEDs both show a further important element of efficiency enhancement. In both cases, the power and current efficiencies of the respective HF-OLEDs are higher compared to the TADF and **ν-DABNA** OLEDs (Figure **S7**, **S8**), only partially explained by the improved quantum efficiency of the HF devices. In **ACRSA**, power and current efficiency rise from 31 cd A^{-1} and 28 lm W^{-1} in the greenish TADF OLEDs to 37 cd A^{-1} and 36 lm W^{-1} in the HF-OLEDs, despite their deep-blue colour coordinate. Similar results with much stronger improvement in efficiency is observed for **AZB-TRZ** HF-

OLEDs, rising from 12 cd A^{-1} and 9 lm W^{-1} in the TADF OLEDs to 30 cd A^{-1} and 27 lm W^{-1} in the HF-OLEDs (Figure **S8**). In contrast, **DMAC-TRZ** HF-OLEDs show a decrease of power efficiency compared to the **DMAC-TRZ** devices because EQE remains unchanged and only the spectrum changes (Figure **S9**). The slightly higher power efficiency values of the **DMAC-TRZ** HF-OLEDs, compared to the other two sensitisers, is attributed to the stronger contribution of **DMAC-TRZ** to the overall EL spectrum (Table **S5**). Indeed, due to physiological response curves a green emitter with similar radiance to a deeper blue emitter is always expected to have higher power efficiency – a trend that the overwhelming efficiency enhancements of our HF OLEDs disrupts.

Conclusions

Here we have investigated the key photophysical parameters that support optimal triplet up-conversion sensitisation for use in HF-OLEDs. We show that these parameters differ considerably from those required for a TADF molecule to exhibit strong performance as an OLED emitter. Importantly, rigid TADF molecules with homogeneity of the CT emission energy, exemplified by the spiro-linked TADF molecule **ACRSA**, allow all molecules in the film to undergo efficient FRET. Additionally, long radiative lifetimes and low ISC rates can be ideal for sensitisation, allowing small spectral overlaps to nonetheless support efficient cumulative FRET to the terminal emitter. Although high rISC rates are desirable for achieving shorter triplet lifetimes and minimising triplet annihilation/quenching phenomena, in HF-OLEDs the k_{ISC} (and consequently the k_{rISC}) must strike a delicate balance between being fast enough to ensure device stability and slow enough to allow FRET to outcompete it. The efficient FRET can then circumvent the moderate PLQY of **ACRSA** and **AZB-TRZ**, in our case also providing narrowband blue emission from **ν-DABNA**. This strategy also enables the sensitiser excitation energies to be pushed as low as possible while retaining deep-blue emission, with significant benefits on choice of host material and device longevity.

These results therefore reveal an interesting ‘blind spot’ in TADF and hyperfluorescence research. By limiting scope to only the ‘best’ performing TADF materials as sensitisers (such as **DMAC-TRZ** previously), it is likely that many excellent hyperfluorescent pairs using ‘less ideal’ TADF sensitisers have been overlooked, and would likely never be considered or discovered. This ability to turn intrinsically ‘poor’ TADF emitters into blue HF-OLEDs with exceptional performance, (Figure **S10**) we suggest should stimulate a re-evaluation of many previously reported and un-reported TADF materials, as well as reassessment of current perceptions of what make novel photonic materials worthy of publication.

References:

1. On the way to becoming the world market leader in the OLED sector. https://www.techtag.de/digitalisierung/digitale-pioniere/cynora-auf-dem-weg-zum-weltmarktfuehrer-im-oled-bereich-interview/.
2. Hong, G. *et al.* A Brief History of OLEDs—Emitter Development and Industry Milestones. *Adv. Mater.* **33**, 2005630 (2021).
3. Samsung Display researching phosphorescent blue OLED material. https://www.thelec.net/news/articleView.html?idxno=4044.
4. Ihn, S. *et al.* Dipole Moment- and Molecular Orbital-Engineered Phosphine Oxide-Free Host Materials for Efficient and Stable Blue Thermally Activated Delayed Fluorescence. *Adv. Sci.* **9**, 2102141 (2022).
5. Wright, I. A. *et al.* Conformational Dependence of Triplet Energies in Rotationally Hindered N- and S-Heterocyclic Dimers: New Design and Measurement Rules for High Triplet Energy OLED Host Materials. *Chem. – A Eur. J.* **27**, 6545–6556 (2021).
6. Aksoy, E., Danos, A., Varlikli, C. & Monkman, A. P. Navigating CIE Space for Efficient TADF Downconversion WOLEDs. *Dye. Pigment.* **183**, 108707 (2020).
7. Monkman, A. Why Do We Still Need a Stable Long Lifetime Deep Blue OLED Emitter? *ACS Appl. Mater. Interfaces* **14**, 20463–20467 (2022).
8. Baldo, M. A., Thompson, M. E. & Forrest, S. R. High-efficiency fluorescent organic light-emitting devices using a phosphorescent sensitizer. *Nature* **403**, 750–753 (2000).
9. Haase, N. *et al.* Are the rates of dexter transfer in TADF hyperfluorescence systems optically accessible? *Mater. Horizons* **8**, 1805–1815 (2021).
10. Nakanotani, H. *et al.* High-efficiency organic light-emitting diodes with fluorescent emitters. *Nat. Commun.* **5**, 4016 (2014).
11. Abroshan, H. *et al.* Thermally Activated Delayed Fluorescence Sensitization for Highly Efficient Blue Fluorescent Emitters. *Adv. Funct. Mater.* **30**, 2005898 (2020).
12. Furukawa, T., Nakanotani, H., Inoue, M. & Adachi, C. Dual enhancement of electroluminescence efficiency and operational stability by rapid upconversion of triplet excitons in OLEDs. *Sci. Rep.* **5**, 8429 (2015).
13. Fukagawa, H., Shimizu, T., Iwasaki, Y. & Yamamoto, T. Operational lifetimes of organic light-emitting diodes dominated by Förster resonance energy transfer. *Sci. Rep.* **7**, 1735 (2017).
14. Hatakeyama, T. *et al.* Ultrapure Blue Thermally Activated Delayed Fluorescence Molecules: Efficient HOMO-LUMO Separation by the Multiple Resonance Effect. *Adv. Mater.* **28**, 2777–2781 (2016).
15. Stavrou, K. *et al.* Emission and Absorption Tuning in TADF B,N-Doped Heptacenes: Toward Ideal-Blue Hyperfluorescent OLEDs. *Adv. Opt. Mater.* 1–21 (2022)

doi:10.1002/adom.202200688.

16. Alam, M. I. *et al.* Acceptor Interlocked Molecular Design for Solution-Processed Stable Deep-Blue TADF and Hyper Fluorescence Organic LED Enabling High-Efficiency. *Adv. Opt. Mater.* **10**, 2200376 (2022).

17. Stavrou, K. *et al.* Unexpected Quasi-Axial Conformer in Thermally Activated Delayed Fluorescence DMAC-TRZ, Pushing Green OLEDs to Blue. *Adv. Funct. Mater.* 2300910 (2023) doi:10.1002/adfm.202300910.

18. Wada, Y., Nakagawa, H., Matsumoto, S., Wakisaka, Y. & Kaji, H. Organic light emitters exhibiting very fast reverse intersystem crossing. *Nat. Photonics* **14**, 643–649 (2020).

19. Kim, J. H., Lee, K. H. & Lee, J. Y. Design of Thermally Activated Delayed Fluorescent Assistant Dopants to Suppress the Nonradiative Component in Red Fluorescent Organic Light-Emitting Diodes. *Chem. – A Eur. J.* **25**, 9060–9070 (2019).

20. Jeon, S. O. *et al.* High-efficiency, long-lifetime deep-blue organic light-emitting diodes. *Nat. Photonics* **15**, 208–215 (2021).

21. Chan, C.-Y. *et al.* Stable pure-blue hyperfluorescence organic light-emitting diodes with high-efficiency and narrow emission. *Nat. Photonics* **15**, 203–207 (2021).

22. Lee, Y. *et al.* Investigating HOMO Energy Levels of Terminal Emitters for Realizing High-Brightness and Stable TADF-Assisted Fluorescence Organic Light-Emitting Diodes. *Adv. Electron. Mater.* **7**, 2001090 (2021).

23. Naveen, K. R. *et al.* Achieving High Efficiency and Pure Blue Color in Hyperfluorescence Organic Light Emitting Diodes using Organo-Boron Based Emitters. *Adv. Funct. Mater.* **32**, 2110356 (2022).

24. Naveen, K. R., Palanisamy, P., Chae, M. Y. & Kwon, J. H. Multiresonant TADF materials: triggering the reverse intersystem crossing to alleviate the efficiency roll-off in OLEDs. *Chem. Commun.* **59**, 3685–3702 (2023).

25. Naveen, K. R., Yang, H. I. & Kwon, J. H. Double boron-embedded multiresonant thermally activated delayed fluorescent materials for organic light-emitting diodes. *Commun. Chem.* **5**, 1–14 (2022).

26. Cheng, Y. *et al.* A Highly Twisted Carbazole-Fused DABNA Derivative as an Orange-Red TADF Emitter for OLEDs with Nearly 40 % EQE. *Angew. Chemie Int. Ed.* **61**, (2022).

27. Stavrou, K., Danos, A., Hama, T., Hatakeyama, T. & Monkman, A. Hot vibrational states in a high-performance multiple resonance emitter and the effect of excimer quenching on organic light-emitting diodes. *ACS Appl. Mater. Interfaces* **13**, 8643–8655 (2021).

28. Naqvi, B. A. *et al.* What Controls the Orientation of TADF Emitters? *Front. Chem.* **8**, 1–11 (2020).

29. Penfold, T. J., Dias, F. B. & Monkman, A. P. The theory of thermally activated delayed fluorescence for organic light emitting diodes. *Chem. Commun.* **54**, 3926–3935 (2018).

30. Kukhta, N. A. *et al.* Revealing resonance effects and intramolecular dipole interactions in the positional isomers of benzonitrile-core thermally activated delayed fluorescence materials. *J. Mater. Chem. C* **7**, 9184–9194 (2019).

31. Tsai, W.-L. *et al.* A versatile thermally activated delayed fluorescence emitter for both highly efficient doped and non-doped organic light emitting devices. *Chem. Commun.* **51**, 13662–13665 (2015).

32. Nasu, K. *et al.* A highly luminescent spiro-anthracenone-based organic light-emitting diode exhibiting thermally activated delayed fluorescence. *Chem. Commun.* **49**, 10385–10387 (2013).

33. Sudhakar, P. *et al.* Azaborine as a Versatile Weak Donor for Thermally Activated Delayed Fluorescence. *ACS Appl. Mater. Interfaces* **15**, 25806–25818 (2023).

34. Stavrou, K., Franca, L. G. & Monkman, A. P. Photophysics of TADF Guest–Host Systems: Introducing the Idea of Hosting Potential. *ACS Appl. Electron. Mater.* **2**, 2868–2881 (2020).

35. Kelly, D., Franca, L. G., Stavrou, K., Danos, A. & Monkman, A. P. Laplace Transform Fitting as a Tool To Uncover Distributions of Reverse Intersystem Crossing Rates in TADF Systems. *J. Phys. Chem. Lett.* **13**, 6981–6986 (2022).

36. Franca, L. G., Danos, A. & Monkman, A. Spiro donor–acceptor TADF emitters: naked TADF free from inhomogeneity caused by donor acceptor bridge bond disorder. Fast rISC and invariant photophysics in solid state hosts. *J. Mater. Chem. C* **10**, 1313–1325 (2022).

37. Franca, L. G., Danos, A. & Monkman, A. Donor, Acceptor, and Molecular Charge Transfer Emission All in One Molecule. *J. Phys. Chem. Lett.* **14**, 2764–2771 (2023).

38. Haase, N. *et al.* Kinetic Modeling of Transient Photoluminescence from Thermally Activated Delayed Fluorescence. *J. Phys. Chem. C* **122**, 29173–29179 (2018).

39. Sem, S. *et al.* Determining non-radiative decay rates in TADF compounds using coupled transient and steady state optical data. *J. Mater. Chem. C* **10**, 4878–4885 (2022).

Methods

Photophysical measurements.

Solid-state samples were evaporated on quartz substrates into a Kurt J. Lesker Super Spectros deposition chamber, at pressures below 10^{-7} mbar. Steady-state absorption and emission spectra were measured using a double beam Shimadzu UV-3600 UV/VIS/NIR spectrophotometer and a Horiba Jobin Yvon Fluorolog-3 spectrofluorometer, respectively. Time-resolved measurements were performed using a spectrograph (Horiba Triax) and a Stanford Computer Optics 4Picos ICCD camera, where samples were excited with a Nd:YAG laser (EKSPLA, 10 Hz, 355 nm) under vacuum.

Device Fabrication.

OLEDs were fabricated on patterned indium tin oxide (ITO)-coated glass (VisionTek Systems) with a sheet resistance of 15 Ω/sq. After sonicating in acetone and isopropanol, oxygen-plasma cleaned substrates were loaded into a Kurt J. Lesker Super Spectros deposition chamber, and both the small molecule and cathode layers were thermally evaporated at pressure below 10^{-7} mbar. The materials used for the production of the OLEDs were N,N-bis(naphthalene-1-yl)-N,-bis(phenyl)benzidine (NPB) as HTL, of 3,3′-Di(9H-carbazol-9-yl)-1,1′-biphenyl (mCBP) as EBL, the EML had 3,3′-di(carbazol-9-yl)-5-cyano-1,1′-biphenyl (mCBPCN) or 1,3-Bis(N-carbazolyl)benzene (mCP) as host, **DMAC-TRZ**, **ACRSA** and **AZB-TRZ** as the sensitiser and **ν-DABNA** as the terminal emitter, 2,4,6-tris(biphenyl-3-yl)-1,3,5-triazine (T2T) as the hole blocking layer (HBL), T2T and 8-hydroxyquinolinolato-lithium (Liq) as the electron transport/injection layer (ETL/EIL), and aluminium (Al) cathode. NPB, mCP, mCBP, and T2T were purchased from SigmaAldrich, mCBPCN and **ACRSA** from Ossila and sublimed before use. Sublimed **DMAC-TRZ** was purchased from Lumtec. **ν-DABNA** was synthesised and purified by Prof. Hatakeyama group. **AZB-TRZ** was synthesised and purified by Eli Zysman-Colman group.

Device Characterization

Freshly evaporated devices were transferred into a calibrated 6-inch integrating sphere (Labsphere) in a glovebox, and their electrical properties were measured using a source meter (Keithley 2400). Emission spectra were simultaneously measured using both a calibrated fiber coupled spectrometer (Ocean optics USB4000) and a photodiode, for low luminance. All devices were evaluated at 293 K and under N2 atmosphere.

Data availability

The data that support the plots within this paper and supporting information and other findings of this study are available from the corresponding author upon reasonable request.

Author contributions

K.S. and A.P.M conceived the idea. K.S. designed the experiments. K.S. performed the photophysics, FRET calculations, device fabrication and analysis. K.S. and L.G.F conducted the time-resolved photoluminescence measurements. A.D. measured the photoluminescence quantum yield. All authors contributed to the discussion, writing and editing of the manuscript. A.P.M. supervised the project.

Acknowledgments

We thank Prof. Takuji Hatakeyama and Prof. Eli Zysman-Colman for providing the **ν-DABNA** and **AZB-TRZ** emitters, respectively. This project has received funding from the European Union’s Horizon 2020 research and innovation programme under the Marie Skłodowska Curie grant agreement No 812872 (TADFlife). APM acknowledges the EPSRC for funding under grant number EP/T02240X/1.

Competing interests

The authors declare no competing interests.